

## **Seismic detection of cracks in carbonates associated with potash mining**

Zimin Zhang and Robert R. Stewart

### **SUMMARY**

Brine inflow in a mine, resulting from cracks or fractures in overlying strata, can be a significant problem. This report investigates whether cracked or fractured rock, associated with potash mining in western Canada, might be detectable by multi-component seismic methods. Rock physics modeling was carried out to simulate cracked rocks overlying a potash ore zone. The Kuster-Toksöz procedure modeled randomly distributed cracks while Hudson's formulation was used for aligned cracks in a carbonate interval (the Dawson Bay including the Second Red Bed Shale) overlying the Prairie Evaporites. We find that cracked rocks can display a significant velocity decrease for both P- and S-velocities. For aligned cracks, velocity anisotropy was also observed. Synthetic seismograms for these cracked media show some character change (time shifts, amplitude variation with offset) compared with uncracked responses. The results provide promise for the detection of cracked rock using multi-component seismic data and repeated surveys.

### **INTRODUCTION**

The middle Devonian Elk Point Group contains the largest volume of salt deposits preserved in the Western Canada Sedimentary Basin. These deposits (Figure 1) extend from the USA northward for more than 1900km (1200 miles) to Canada's Northwest Territories (DeMille *et al.*, 1964). In the study area (outlined by the dashed line in Figure 1), the most widely developed of such deposits is the Prairie Evaporite Formation, which is present through much of the Williston Basin region. Its thickness ranges from 0 to about 220m. Potash ore (used as fertilizer and other products) is situated 20-30m from the top of a 100-200m thick salt unit, approximately 960m below the surface. Mining is undertaken using a long room and pillar method. The ore body is 30m thick on average with a typical composition of 55% halite, 40% sylvite, 4% carnallite and 1% insolubles (Maxwell *et al.*, 2005). A generalized stratigraphic column for the area is shown in Figure 2.

A major problem for potash mining in this area can be brine inflow. This may cause ore loss and operational or personnel problems. There are two situations associated with brine movement: flows or dissolution before mining and inflows during mining. The existence of brine prior to mining can cause disruption to normal Phanerozoic stratigraphy by way of collapse structures. Collapse structures are localized regions of considerable, sometimes complete, removal of original geological layering and resultant overlying collapse. These features are thought to result from the dissolution of Prairie Evaporite salts, with associated brecciation and collapse of the overlying (mostly carbonate, then shale) strata into the washout caverns (e.g. Gendzwill and Lundberg, 1989). Collapses are often assumed to take the shape of sub-vertical cylinders, 100m to 1000m in diameter, extending from depth of over 1000m possibly to the surface. Mining

into one of these collapse zones could result in cost increases for the mining operation at best, and in some instances the loss of the mine (Prugger et al., 2004).



FIG. 1. Areal distribution of potash-bearing rocks in the Elk Point Basin (from Fuzesy, 1982).

The use of the long-room and pillar mining method may cause subsurface stress fields to change, thus potentially inducing cracks. In the potash mining area, there can be an aquifer at the bottom of the Souris River Formation (Figure 2). Between the aquifer and ore zone, the formation is composed of shale, dolomite and dolomitized limestone. All these rocks are apt to be cracked. Any fracturing of normally impermeable carbonate rocks could create a brine inflow path that might compromise potash mining operations.

An effective way to mitigate the risk posed by brine flows is to map and predict the volume and location of potentially affected areas prior to mining. 3D seismic surveys have been successfully used to map the subsurface, including collapse structures, for some years in the area. For predicting cracks induced by mining processes, multi-component and repeated (time-lapse) seismic methods might be useful. In this study, rock-physics modeling for cracked media (Appendix) was used to assess the feasibility of detecting cracks by multi-component and time-lapse seismic methods. Kuster-Toksöz modeling (Kuster and Toksöz, 1974) was undertaken to simulate randomly distributed cracks while Hudson's model (Hudson, 1981) was used for aligned cracks. In this study, data and results from two wells are shown: Well A and Well B. Well A is particularly useful as it reaches down to the Cambrian. Well B is within the studied mining area.

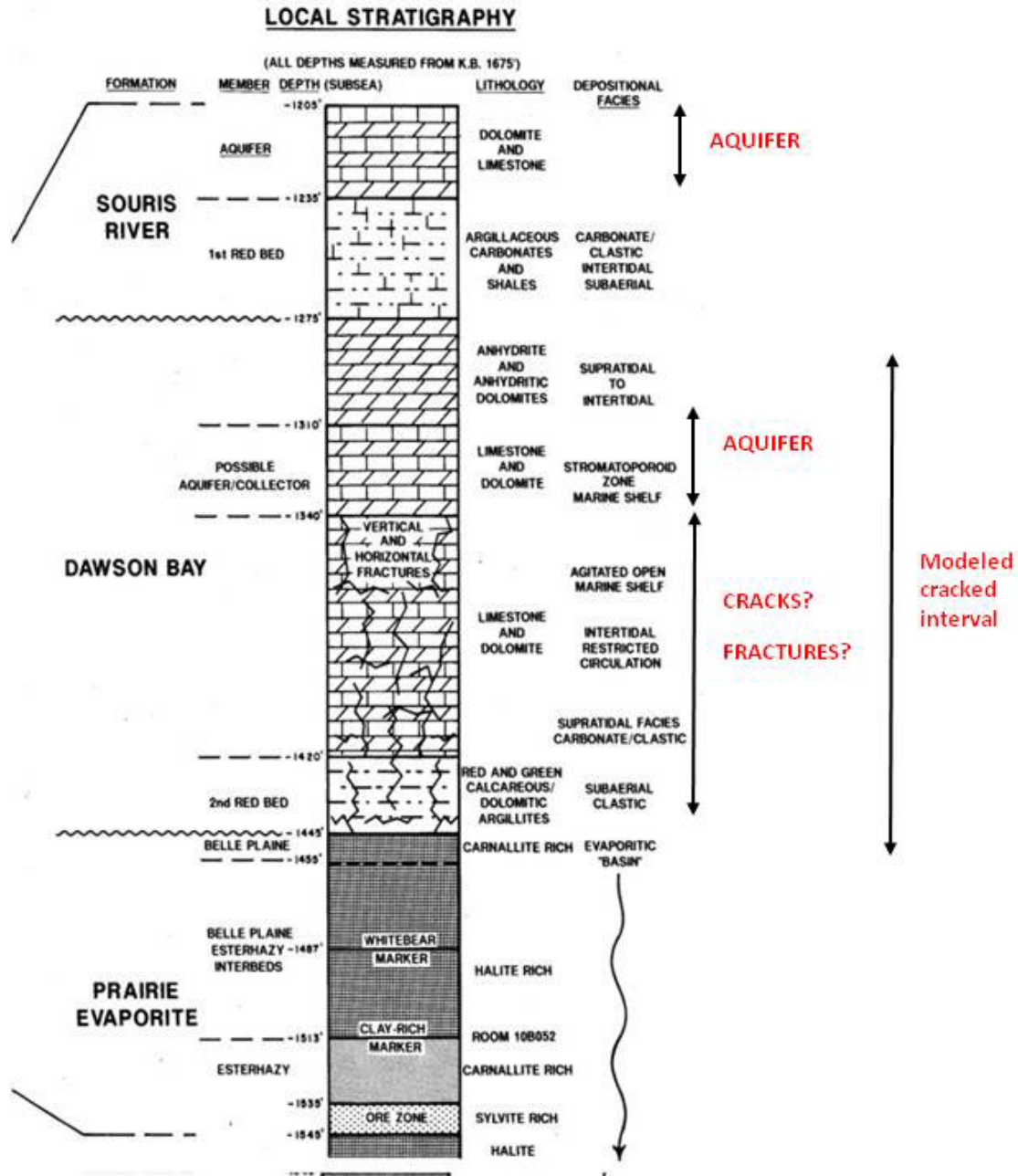


FIG. 2. Local stratigraphy of Prairie Evaporite and overlying formations in the mining area. The Dawson Bay carbonates, dolomites, and shales can host fractures (from R. Edgecombe, personal communication, 2008).

### WELL LOG ANALYSIS AND PROPERTIES OF POTASH ORE

Table 1 shows the well log properties of the minerals for some of the lithologies involved in the study. The essential wireline logs to differentiate the potash ore from other lithologies are the spectral gamma ray and neutron logs. Potash ore displays high radioactivity due to the potassium-40 isotope existing in sylvite (KCl). Sylvite's gamma ray value is about 730 API. Additionally, the ore will display a slightly higher neutron-porosity compared with pure sylvite due to presence of water in carnallite (KCl, MgCl<sub>2</sub>,

6H<sub>2</sub>O). For a typical composition, the gamma ray of the potash ore is about 290 API, the neutron porosity will be in the vicinity of 0%. Figure 3a shows logs from Well A. The Prairie Evaporite is about 150m thick at depth 1010m. The Prairie Evaporite displays overall low neutron-porosity (-5%) and high density-porosity (40%). The ore interval is situated at about 10m from the top of Prairie Evaporite and composed of several thin ore beds. It is about 50m thick. The ore beds display high radioactivity. On the neutron-porosity log, the ore beds generally show a little higher value. Deviation of the neutron-porosity values from the normal trend might be caused by the variation of carnallite content in the ore: carnallite-rich ore displaying a higher neutron-porosity and vice versa (Figure 3b). Sonic velocities in the Paleozoic interval are in the area of 5000m/s for P wave and 2900m/s for S-wave. Vp/Vs values are around 1.8.

Table 1. Well log properties of selected minerals (from Crain, 2005)

	<b>Neutron-porosity (fractional)</b>	<b>DENSITY (kg/m<sup>3</sup>)</b>	<b>Acoustic slowness (μs/m)</b>	<b>PE</b>
<b>Clean Quartz</b>	-0.028	2650	182	1.82
<b>Calcite</b>	0	2710	155	5.09
<b>Dolomite</b>	0.005	2870	144	3.13
<b>Anhydrite</b>	0.002	2950	164	5.08
<b>Fluorite</b>	-0.006	3120	150	6.66
<b>Halite</b>	-0.018	2030	220	4.72
<b>Sylvite</b>	-0.041	1860	242	8.76
<b>Carnallite</b>	0.584	1560	256	4.29

Figure 4 displays the log curves of well B, which is within the mining area under investigation. The Prairie Evaporite is overlain by the 2<sup>nd</sup> Red Bed Shale of the Dawson Bay formation, which is largely dolomite and dolomitized limestone. Above the Dawson Bay lies the 1<sup>st</sup> Red Bed shale and a porous zone which belongs to Souris River Group and is saturated by water. The aquifer is about 15m thick, with quite high porosity, about 20%. Upper Dawson Bay is another aquifer within Dawson Bay, approximately 10m thick with porosity about 16%. The rock layers between the aquifer and Prairie Evaporite consist of shale, dolomite and dolomitized limestone. They are all apt to be cracked. Horizontally and vertically aligned cracks may exist in the Dawson Bay formation. If cracks occur in these formations prior to or during mining process, brine in the aquifer could flow into the mining interval. Thus, it is necessary to identify where the cracks could occur.

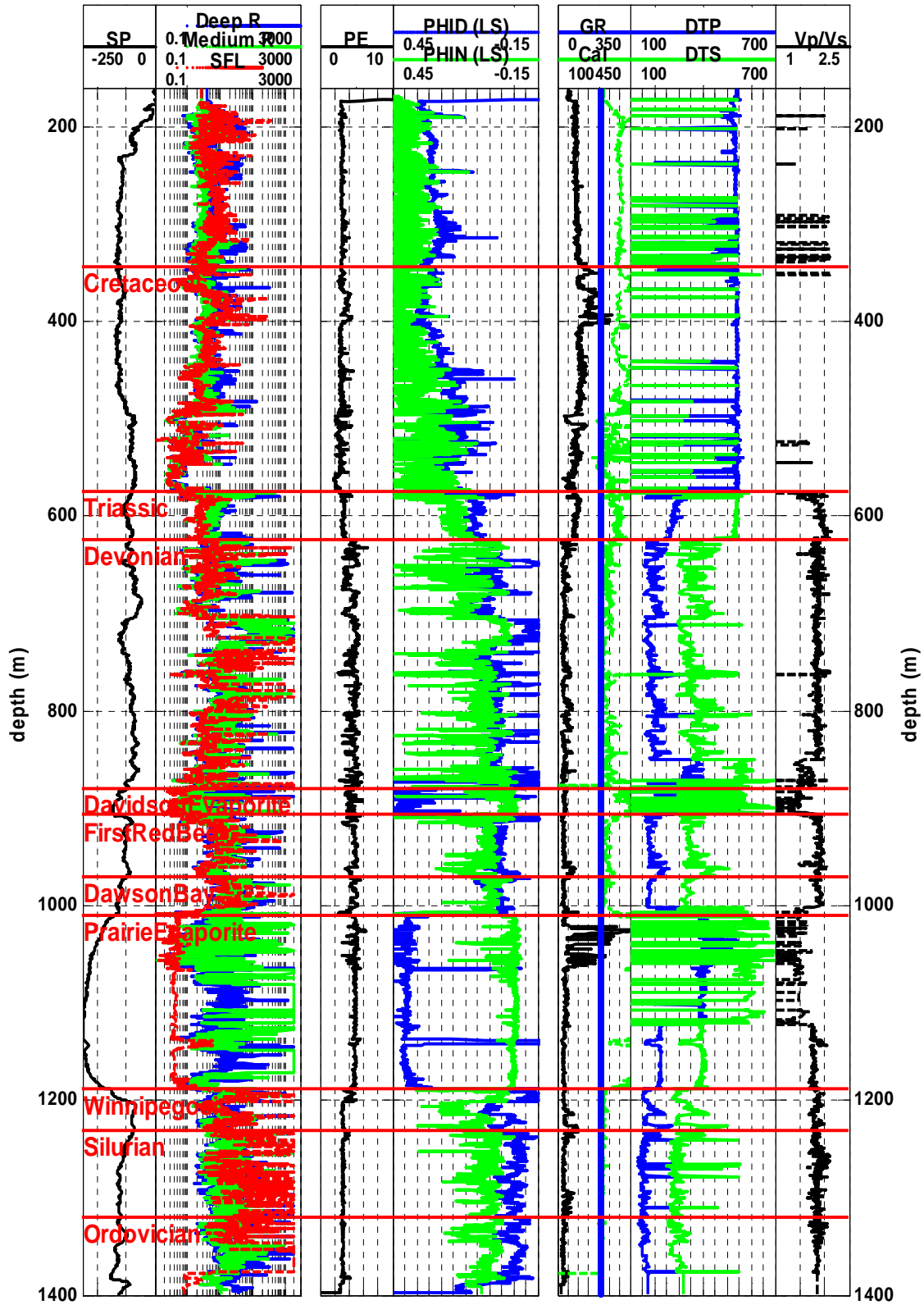


FIG. 3a. Log curves from Well A.

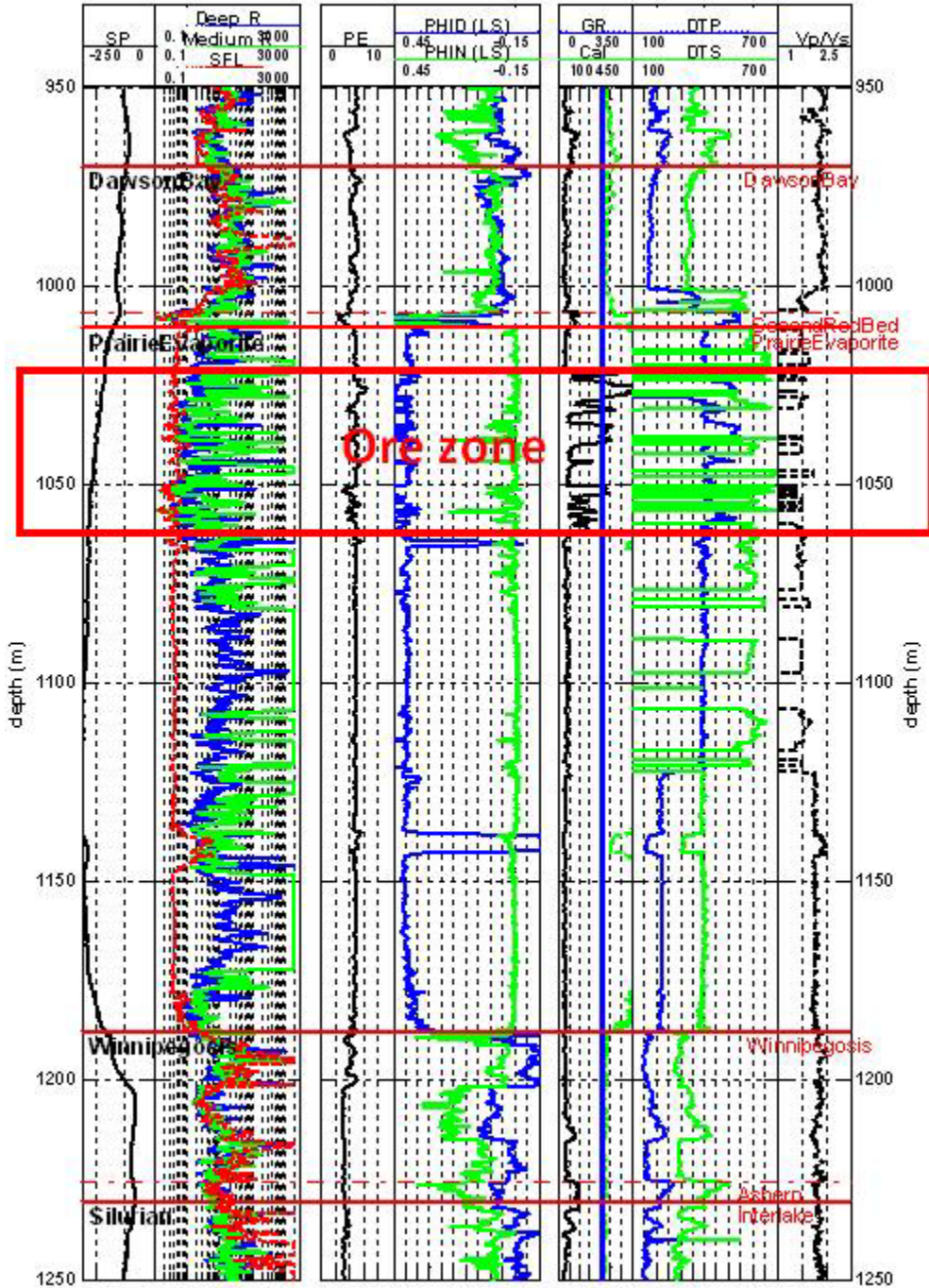


FIG. 3b. Log curves of Well A (as in FIG. 3a), now focusing on the Prairie Evaporite interval.

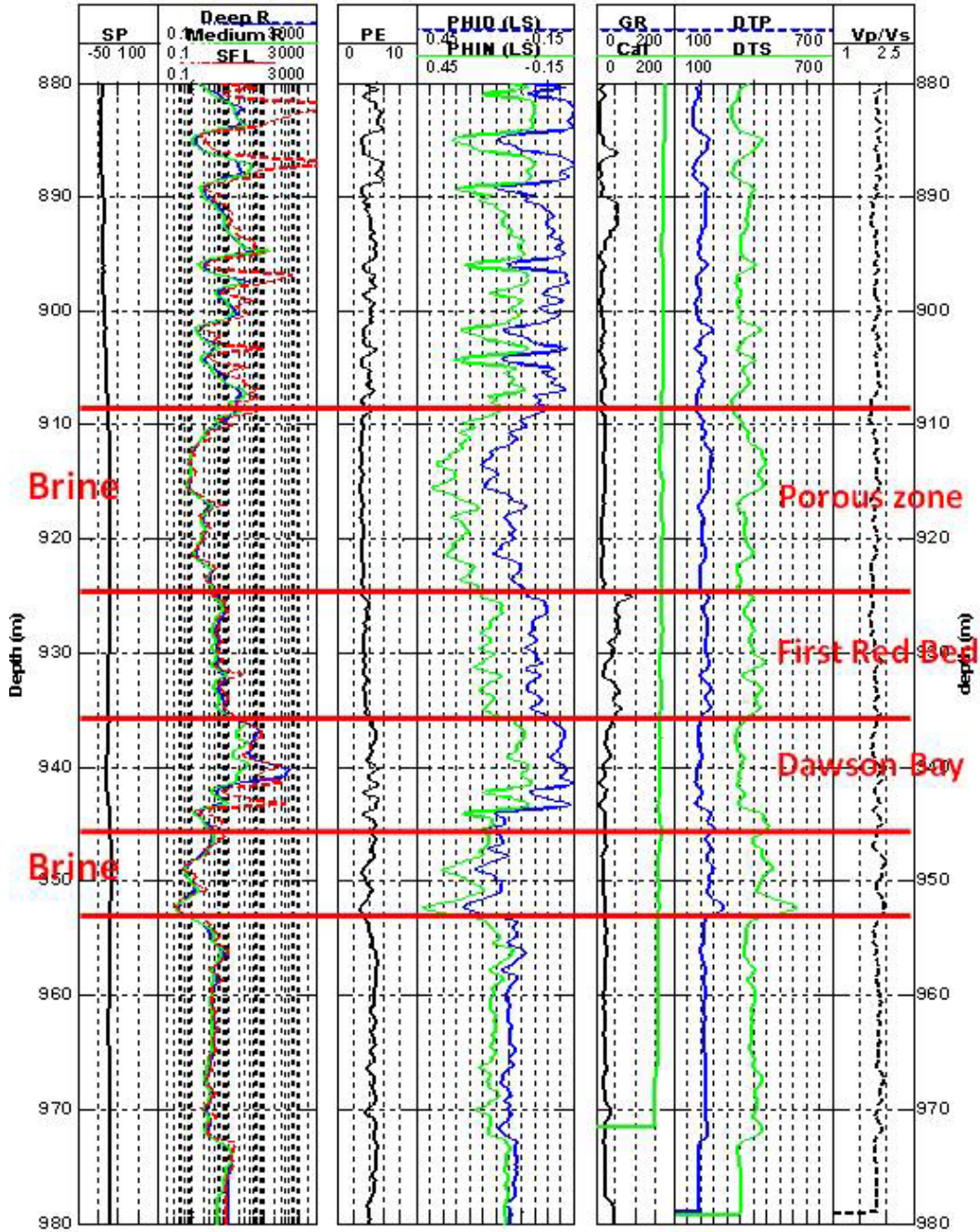


FIG. 4. Logs for Well B.

### ROCK PHYSICS MODELING FOR CRACKED MEDIA

In the potash mining area, an aquifer exists in the Souris River Formation (Figure 2). Just below the aquifer lies the First Red Bed Shale and the Dawson Bay. All these formations, together with the 2<sup>nd</sup> Red Bed Shale above the Prairie Evaporite, can be cracked. To investigate possible elastic changes caused by cracks in these formations, rock physics modeling for cracked media was applied (the full Dawson Bay, including Second Red Bed shale. In Well A, this amounts to a 40m interval while in Well B area, it

is 43m.). The Kuster-Toksöz (1974) method was used for randomly oriented cracks and Hudson's (1981) model was used for aligned cracks. The randomly oriented cracks display overall isotropy, while aligned cracks will introduce anisotropy. Both the Kuster-Toksöz and Hudson's methods assume isolated cracks, thus they are only valid at high-frequencies. For low-frequency moduli calculation, dry moduli were first predicted using effective moduli theory for cracked media. Then, the saturated moduli were calculated through fluid substitution using the Gassmann equation for randomly distributed cracks. Because aligned cracks induce anisotropy, the effective saturated moduli were calculated using Brown and Korringa's (Brown and Korringa, 1975) low-frequency relations.

The sequence for modeling fractures and cracks is:

- 1) Edit the well log values (especially shear logs);
- 2) Predict shear logs using P-velocity and density logs where the shear log is not reliable;
- 3) Model dry cracks using the Kuster-Toksöz method and undertake fluid substitution using Gassmann equation for randomly oriented cracks;
- 4) Model dry cracks using Hudson's theory and fluid substitution using Brown-Korringa's low frequency relation for aligned cracks;
- 5) Calculate P- and S-velocities for cracked media.

### **Predicting shear velocity from density and P-velocity**

Before modeling the cracked media with values from well logs, it is necessary to investigate the quality of those logs. From Figure 3, we can see poor shear-wave velocities in the shallow part of the well, Davidson Evaporite, and Prairie Evaporite intervals. The P-wave velocity and density log are reasonable. Following the method proposed by Han and Batzle (2004), the shear wave modulus can be predicted from P-wave velocity and density. The coefficients in equation (1) were calculated using the data over the interval with reasonable shear log values (depths 600m-1378m and with positive velocity values):

$$\mu = 0.0 * M^2 + 0.2687 * M + 1.7864, \quad (1)$$

where,  $\mu$  is the shear modulus and  $M$  is the P-modulus ( $M = \rho v_p^2 = K + \mu * 4/3$ .  $\rho$ : density, g/cm<sup>3</sup>;  $v_p$ : P velocity, km/s.).

Figure 5 displays the cross-plot between actual shear velocity from the dipole sonic log and our predicted shear velocity. A reasonable correlation can be seen (with a correlation coefficient of 0.99). Figure 6 also shows the predicted and actual shear velocity logs and their differences, which are mostly within 200m/s. All the shear velocities over the questionable intervals will be replaced by the predicted values using equation (1).



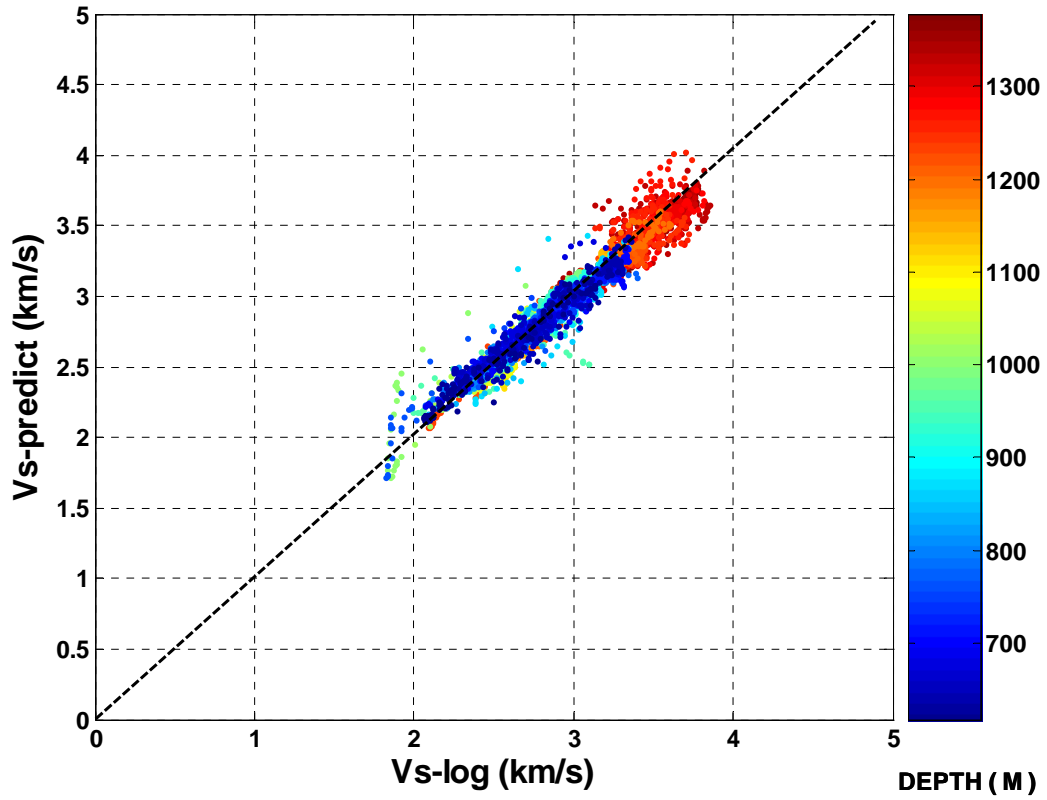


FIG. 5. Comparison of predicted and actual Vs (using M from Vp and  $\rho$ ) for Well A (over depths 600m-1378m with positive velocity values).

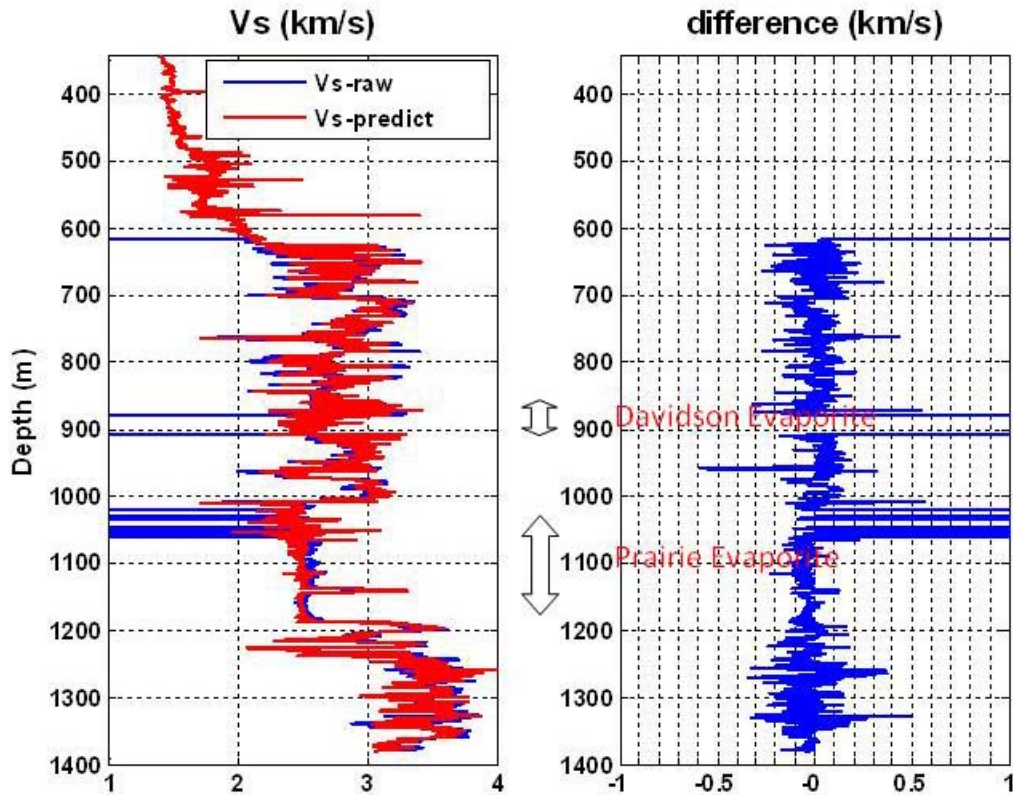


FIG. 6. Predicted (red) and actual Vs (blue) and their difference for Well A.

### Modeling randomly oriented cracks

We first use the Kuster-Toksöz theory (Kuster and Toksöz, 1974; Berryman, 1980) to calculate the effect of cracks in velocities. Some basic definitions of cracks are outlined in Appendix. For crack modeling, we assume that the porosity introduced by cracks is 1%, the aspect ratio is 0.01, and the cracks are penny-shaped. Figure 7 displays the modeled logs of Well A using Kuster-Toksöz model for randomly oriented brine saturated cracks. The density and P-velocity of brine are set to be  $1.1\text{g/cm}^3$ ,  $1430\text{m/s}$  respectively. The P-velocity drops about  $0.7\text{km/s}$  (12.5%), and the shear velocity decreases by  $0.6\text{km/s}$  (20%). For a 40m cracked interval, this amounts to about a 2ms push down in P waves and 3.5ms delay in PS reflection traveltime.

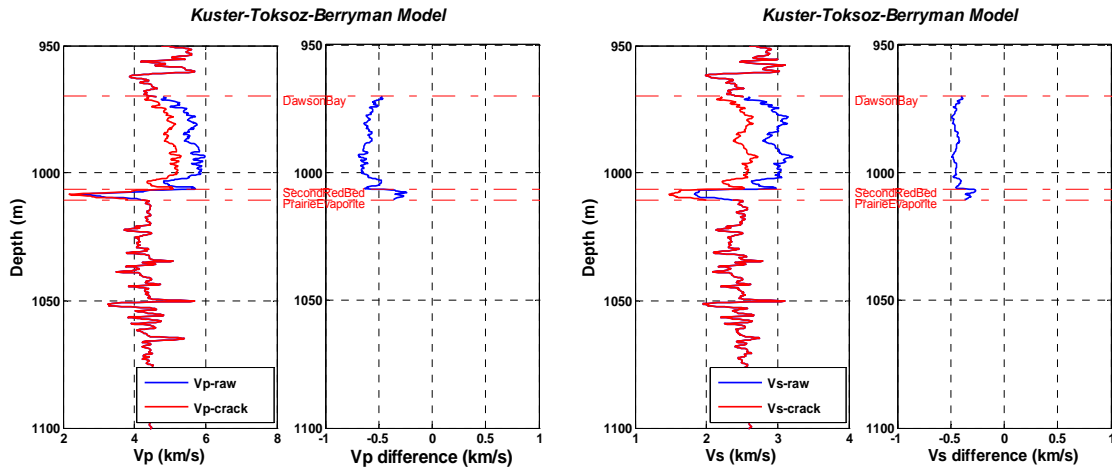


FIG. 7. Velocity of cracked media from Kuster-Toksoz model and velocity difference between uncracked (blue curve) and cracked (red curve) rock for Well A. Left: P-wave velocity; right: shear-wave velocity.

### Modeling vertical aligned cracks

If the cracks are aligned with specific directions (see Figure 8), the elastic properties of rock can be modeled by Hudson's (1981) theory, and the rock will display anisotropy.

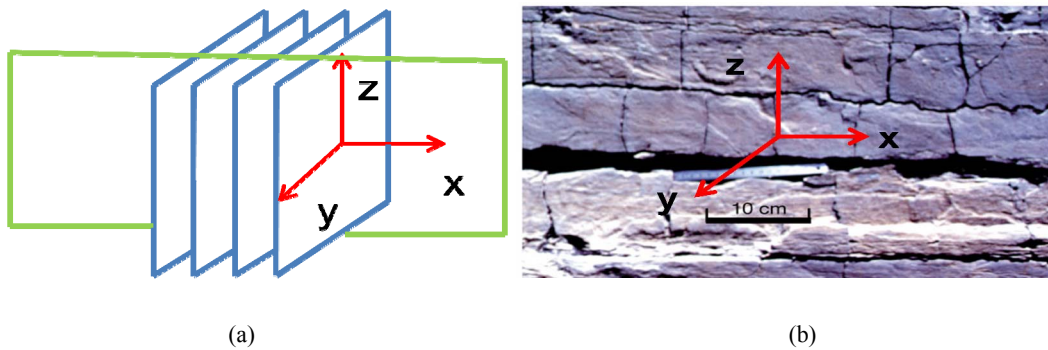


FIG. 8. Schematic diagrams of vertical cracks (a, shown in blue, velocities are modeled assuming waves travel in green plane.) and vertically & horizontally aligned cracks (b: [www.nature.com/.../n6771/images/403753aa.2.jpg](http://www.nature.com/.../n6771/images/403753aa.2.jpg))

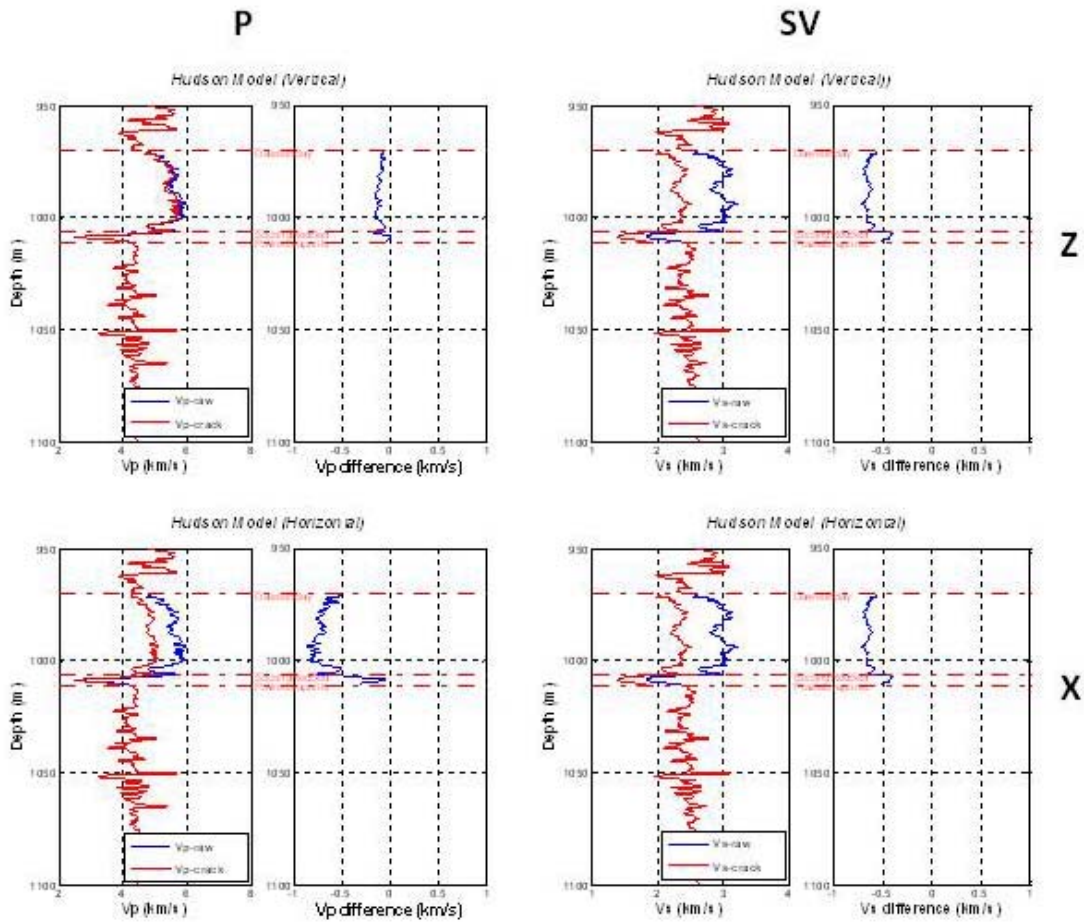


FIG. 9. Top: vertical propagation velocity of a vertically cracked medium from Hudson's formulation and the velocity difference between uncracked and cracked rock (Left: P wave; right: S-wave) for Well A. Bottom: the same plots for horizontally propagating waves through a vertically cracked medium.

Figure 9 shows the modeled logs of Well A assuming vertically aligned cracks in the formations overlying the mining interval. The rock displays transverse isotropy with respect to x direction or azimuthal anisotropy in the x-y plane. The P-velocity along the vertical direction shows a small decrease, less than 0.2km/s (3.5%), while the SV-velocity propagating vertically drops significantly, about 0.8km/s (26%). For horizontally traveling waves, the P-velocity decreases by about 0.75km/s (13.5%) and the SV-velocity drops at the same amount as vertical propagation.

Figure 10 shows the velocity variation with angle from the symmetry axis (the x axis). The P-velocity will gradually drop at small incidence angle from  $0^\circ$  to  $45^\circ$ , and then increase from  $45^\circ$  to  $90^\circ$  incidence. The SV-wave velocity reaches its minimum at 0 and 90 degree incidence, and maximizes at a  $45^\circ$  incidence. The SH-wave velocity drops gradually from vertical to horizontal propagation.

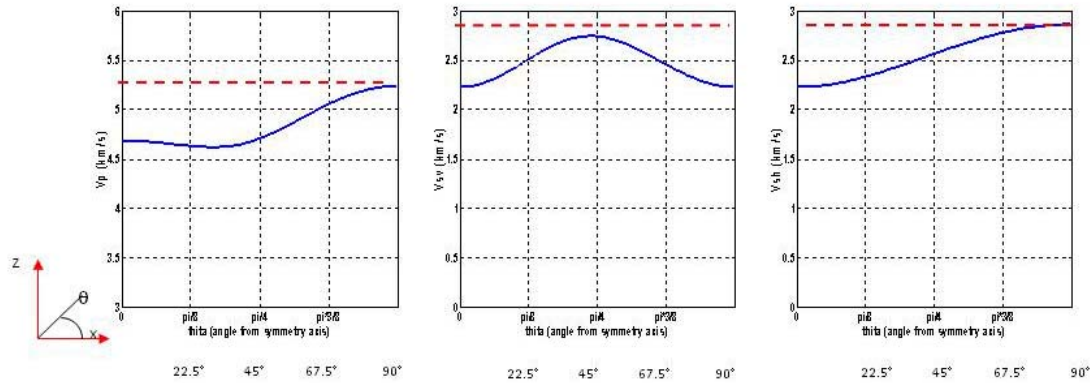


FIG. 10. P- (left), SV- (middle) and SH- (right) velocity variation with angle ( $\theta$ ) from the symmetry axis (x-axis) for the cracked medium. The rock properties of uncracked media (velocities shown by red line in each plot) are the average over Dawson Bay and the Second Red Bed Shale of Well A.

### Modeling vertically and horizontally aligned cracks

There could be two sets of cracks in the rock of Dawson Bay, one of which is aligned in the vertical direction and the other is in the horizontal direction (see Figure 8b). This crack system can be modeled with Hudson's theory and will display azimuthal anisotropy. We assume the total porosity induced by these two set of cracks is still 1%, the aspect ratio is 0.01, and the cracks are penny-shaped. Figure 11 shows the modeled P- and S-velocities for Well A. For vertically propagating P- and S-waves, the velocities will significantly drop. The velocity decrease is about 0.5km/s (about 10%) for the P wave, and 0.75km/s (25%) for the SV wave. The velocities for waves propagating horizontally in the XZ plane are similar to that of vertically travelling waves. However, the horizontal traveling velocities in YZ plane are quite different. Both the P- and SV-velocities drop less than the previous two cases, 0.2km/s (3.5%) for P-wave and 0.35km/s (11.5%) for SV-wave. The velocity variations with incidence angle (from the z-axis) are shown in Figure 12. All the velocities show different variations with angle when traveling in XZ and YZ planes. P- and SV-velocities drop more in the XZ plane than in YZ plane. SH-velocity shows no anisotropy in the XZ plane, but anisotropy is apparent in YZ plane.

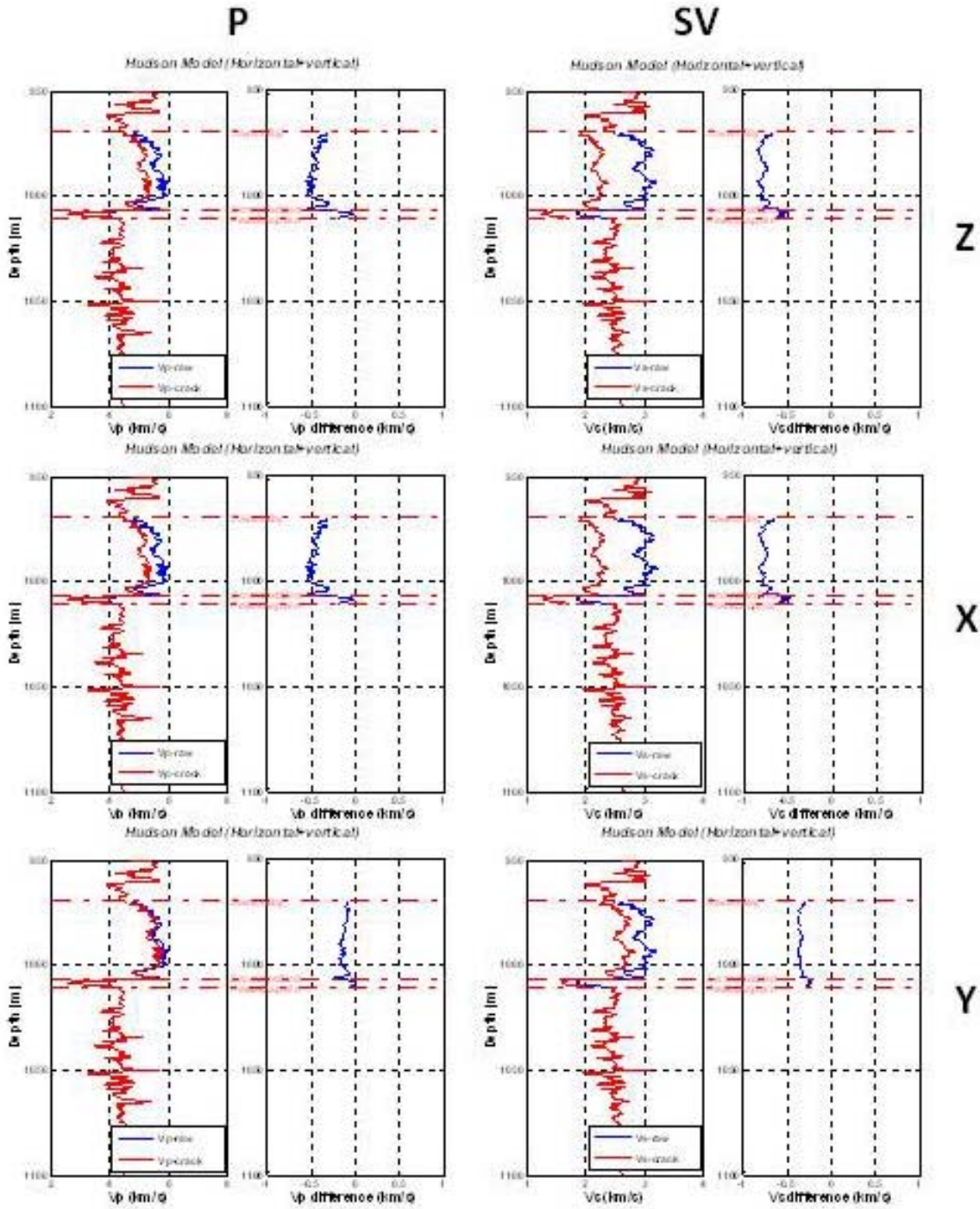


FIG. 11. Modeled velocities and velocity difference between uncracked and cracked rock for vertically and horizontally aligned cracks (Left: P wave; right: SV wave) for Well A. Top: vertically propagating waves; middle: horizontally propagating waves in XZ plane; bottom: horizontally propagating waves in YZ plane.

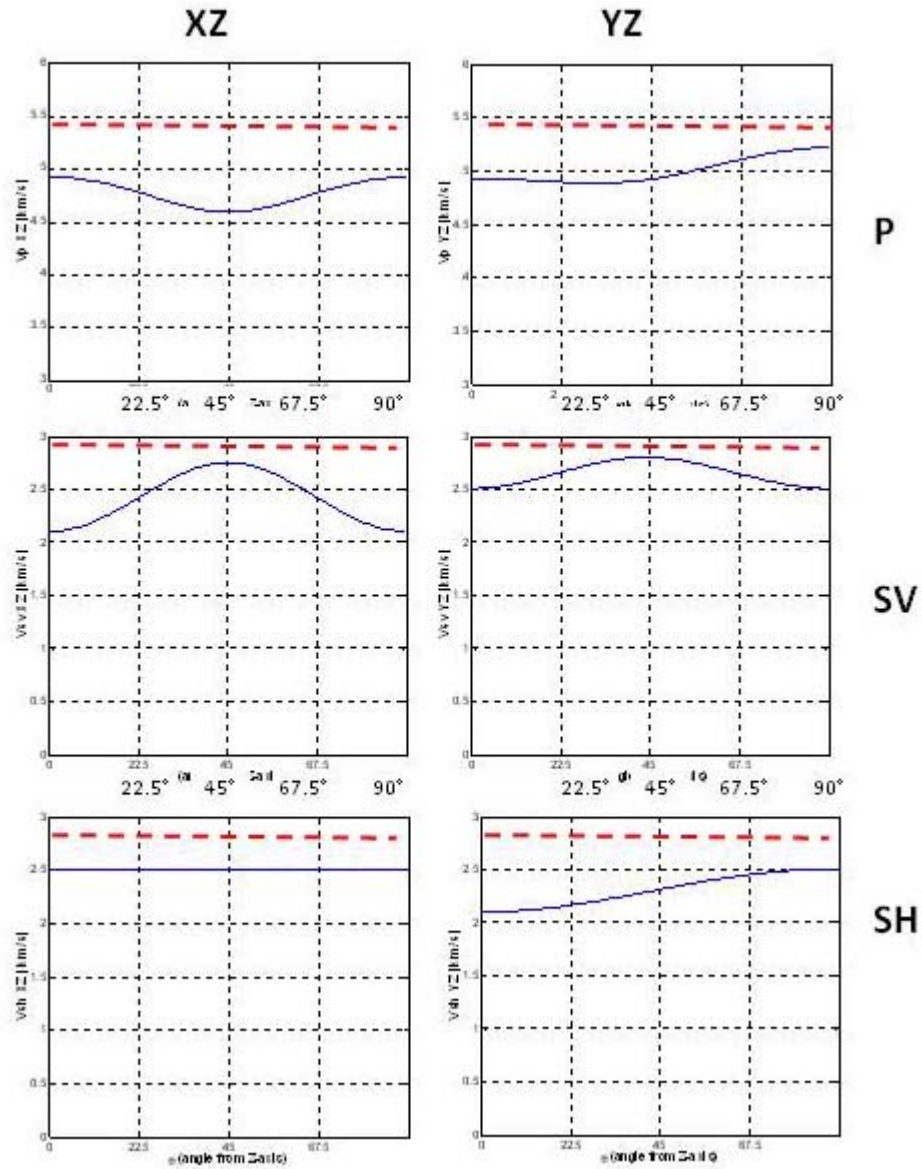


FIG. 12. P- (top), SV- (middle) and SH- (bottom) velocity variation with angle from z-axis for media with horizontally and vertically aligned cracks, the left side is for the wave propagating in the XZ plane and the right is for the wave propagating in YZ plane. The rock properties of uncracked media (velocities shown by red line in each plot) are the average over Dawson Bay and the Second Red Bed Shale of Well A. The Z-axis is in the vertical direction and the X-axis is in the horizontal direction which is normal to vertical cracks.

Table 2. Rock properties for uncracked and cracked rock. The values of matrix for modeling are the averages over the Dawson Bay and Second Red Bed Shale in Well A. The density and P-velocity of brine are set to be 1.1g/cm<sup>3</sup>, 1430m/s. Vert: vertically propagating waves; Hxz: waves travelling horizontally in the XZ plane; Hyz: waves travelling horizontally in the YZ plane. Random: randomly oriented cracks; Vert.: vertically aligned cracks; Vert.+Hor.: vertically & horizontally aligned cracks.

		Matrix	Dry crack			Water saturated crack			
			Random	Vert.	Vert.+Hor.	Random	Vert.	Vert.+Hor.	
Dawson Bay (970.1-1006.5 m)	Density	2683.4	2656.6			2667.6			
	Vp	Vert		-	3851.9	5437.7	5069.3		
		Hxz	5514.7	3980.9	-	3851.9	4926.2	5012.4	5069.3
		Hyz		-	5073.9	-	5390.7		
	Vsv	Vert	2941.7	2499.4	2175.6	2301.1	2171.1		
					(XZ)		(XZ)		
		2595.6			2494.2	2590.2			
(YZ)		(YZ)							
Hxz	-	2175.6	2301.1	2171.1					
Hyz	-	2595.6	-	2590.2					
2 <sup>nd</sup> Red Bed Shale (1006.5-1010.7 m)	Density	2250.4	2227.9			2238.9			
	Vp	Vert		-	2538.2	3545.2	3495.0		
		Hxz	3609.1	2650	-	2538.2	3330.1	3125.7	3495.0
		Hyz		-	3368.0	-	3585.4		
	Vsv	Vert	1984.8	1681.4	1460.9	1677.3	1457.3		
					(XZ)		(XZ)		
		1748.3			1551.9	1744.0			
(YZ)		(YZ)							
Hxz	-	1460.9	1551.9	1457.3					
Hyz	-	1748.3	-	1744.0					



Table 2 gives the values for the Dawson Bay formation. The matrix values for modeling are the averages of Dawson Bay from Well A. Three cases of cracks were modeled: randomly oriented cracks, vertically aligned cracks, and vertically & horizontally aligned cracks. Density and velocities for both dry and water-saturated (brine density  $1.1\text{g/cm}^3$ , P-velocity  $1430\text{m/s}$ ) cracks were calculated. Generally, we find that there is a substantially drop in P-wave and S-wave velocity with cracking. In addition, the amount of this decrease can depend significantly on crack orientation with respect to the seismic wave propagation (azimuthal seismic anisotropy).

The same work was also carried out for Well B. Figure 13 and Figure 14 show the modeled well logs of vertically aligned and vertically plus horizontally aligned cracks for Well B, which is located within the mining area. This modeling gives similar results as for Well A.

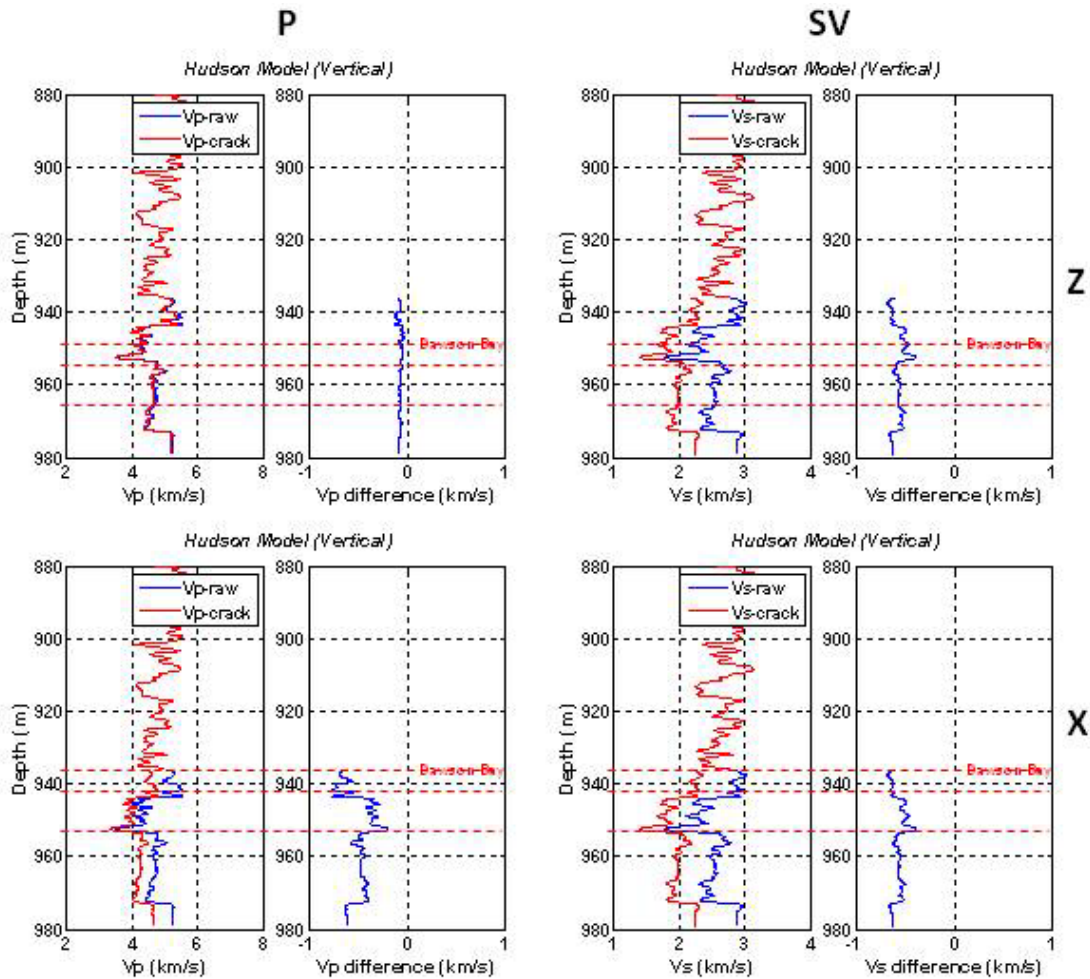


FIG. 13. Top: vertical propagation velocity from Hudson’s model and velocity differences between uncracked and vertically aligned cracks rock (Left: P wave; right: shear wave) for Well B. Bottom: the same plots for horizontally propagating waves.

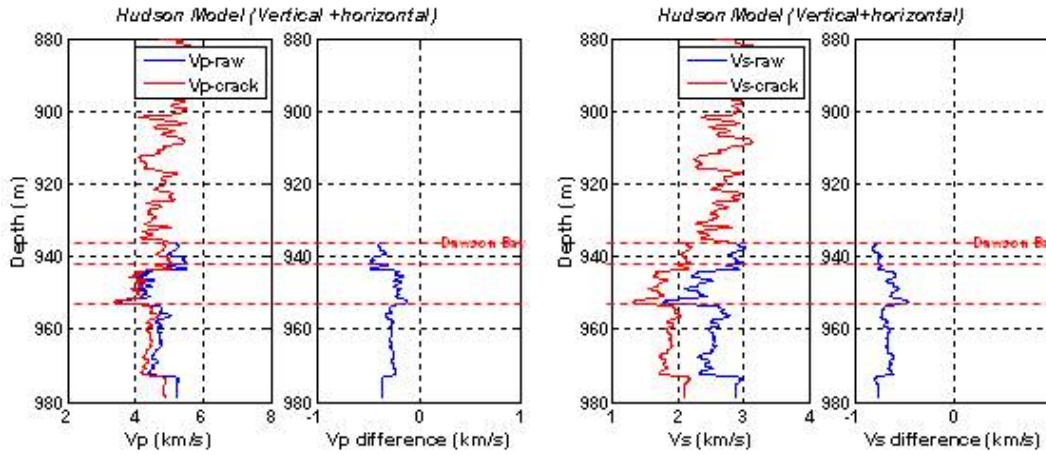


FIG. 14. Vertical propagation velocity from Hudson’s model and velocity differences between uncracked and vertically & horizontally aligned cracks rock (Left: P wave; right: shear wave) for Well B.

**SYNTHETIC SEISMOGRAMS FOR P- AND CONVERTED WAVES**

We now use these “cracked” and uncracked logs to generate synthetic seismograms. The purpose of this simulation is to investigate the change in the seismograms caused by the cracks. Figure 15 shows the Ricker wavelet used (based on the likely bandwidth of field seismic energy). Synthetic seismograms calculated from our modeled velocities and densities for vertically aligned cracks are first illustrated.

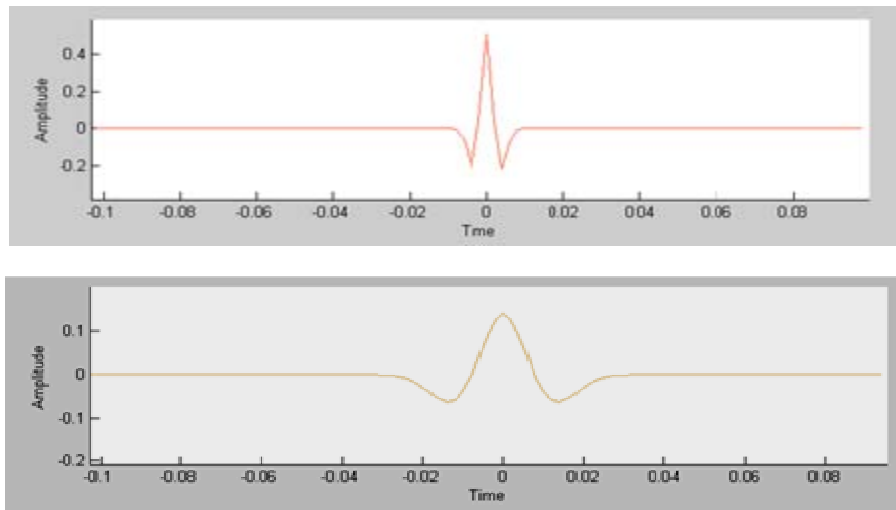


FIG. 15. Ricker wavelet used for synthetic PP (left, dominant frequency 106Hz) and PS (right, 28.85Hz) seismograms.

The software used for synthetic seismogram generation assumes isotropic velocities, so vertical velocities from Hudson’s model were used. Figures 16 through 19 show the original well logs and their accompanying synthetic seismograms along side the “cracked” well logs and their synthetic seismic response.

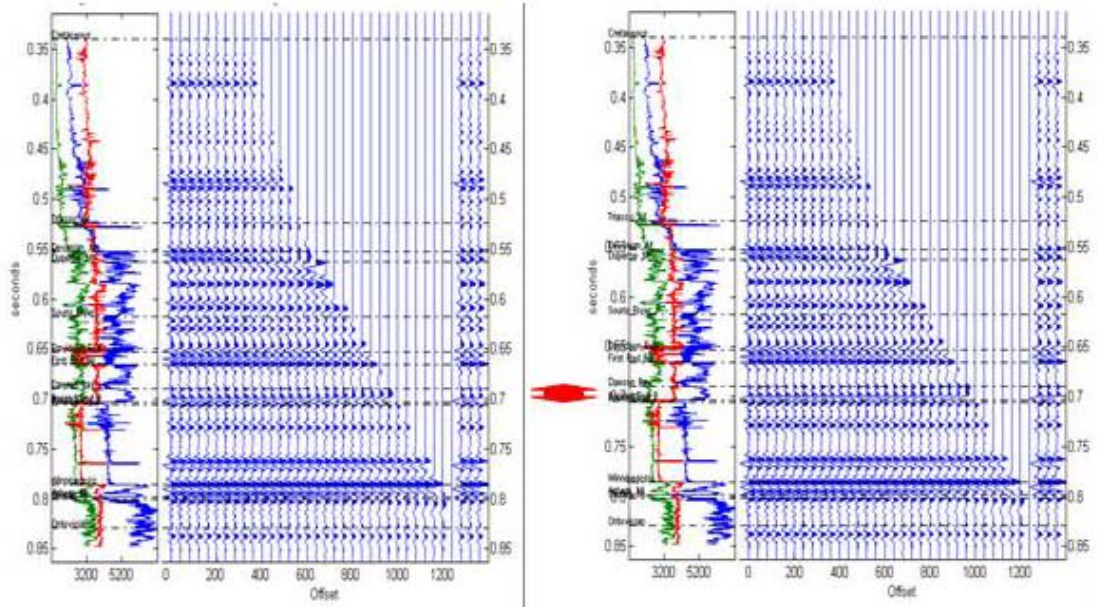


FIG. 16. Well logs (P velocity in blue, S-velocity in green, and density in red) and PP synthetic seismogram (NMO removed gather and summed response, duplicated 3 times) for Well A. Left: uncracked rock; right: cracked rock. The red arrow marks the strata cracked.

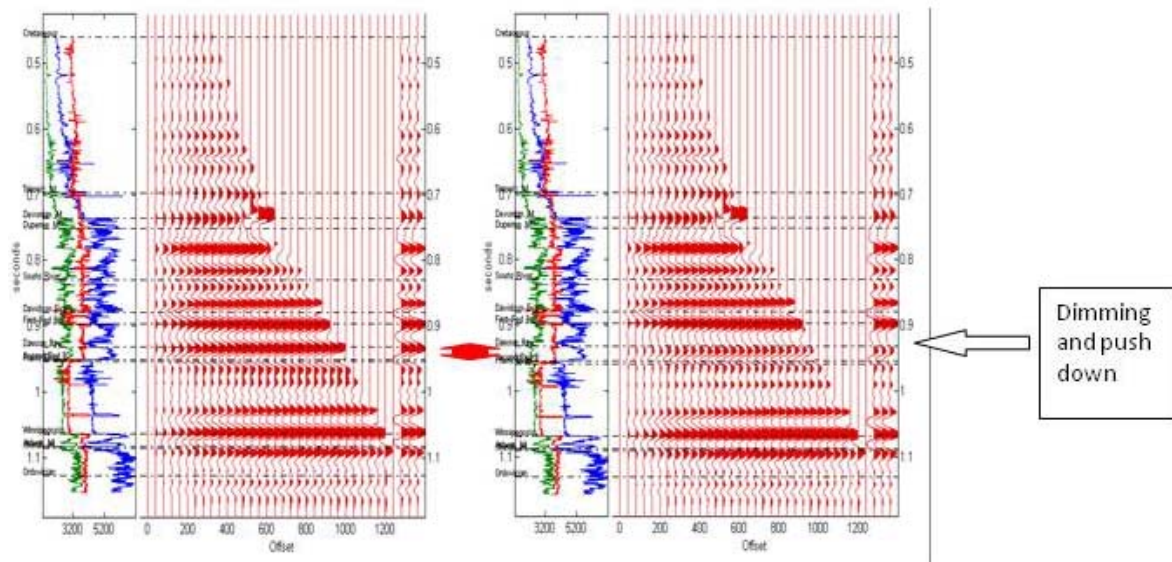


FIG. 17. Well logs (P velocity in blue, S-velocity in green, and density in red) and PS synthetic seismogram (NMO removed gather and summed response, duplicated 3 times) for Well A. Left: uncracked rock; right: cracked rock. The red arrow marks the strata cracked.

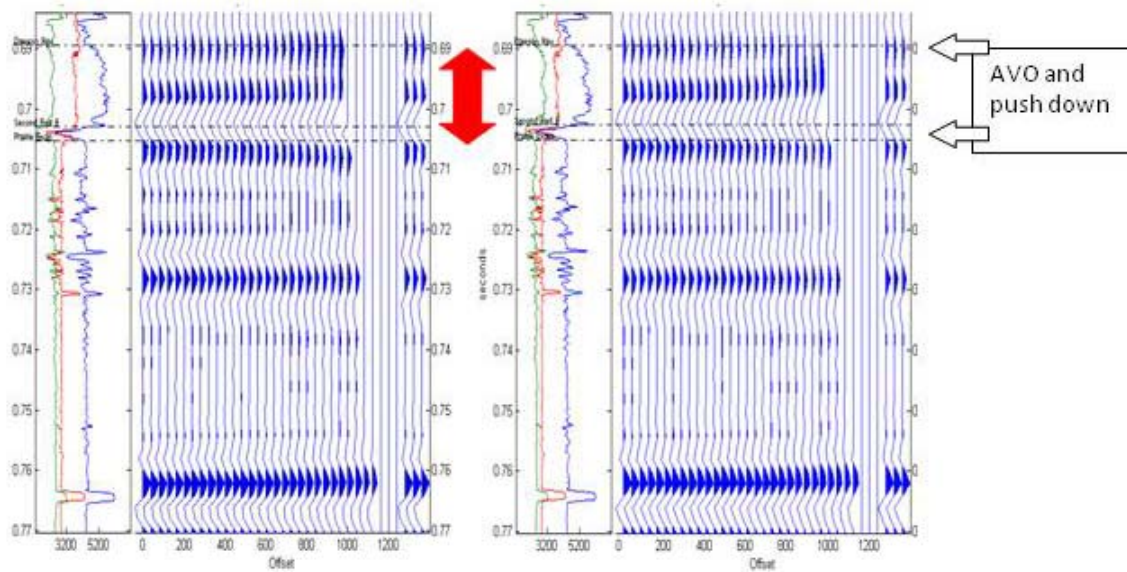


FIG. 18. Well logs (P velocity in blue, S-velocity in green, and density in red) and PP synthetic seismogram (NMO removed gather and summed response, duplicated 3 times) focusing on Dawson Bay and the Second Red Bed Shale for Well A. left: uncracked rock; right: cracked rock. The red arrow marks the strata cracked.

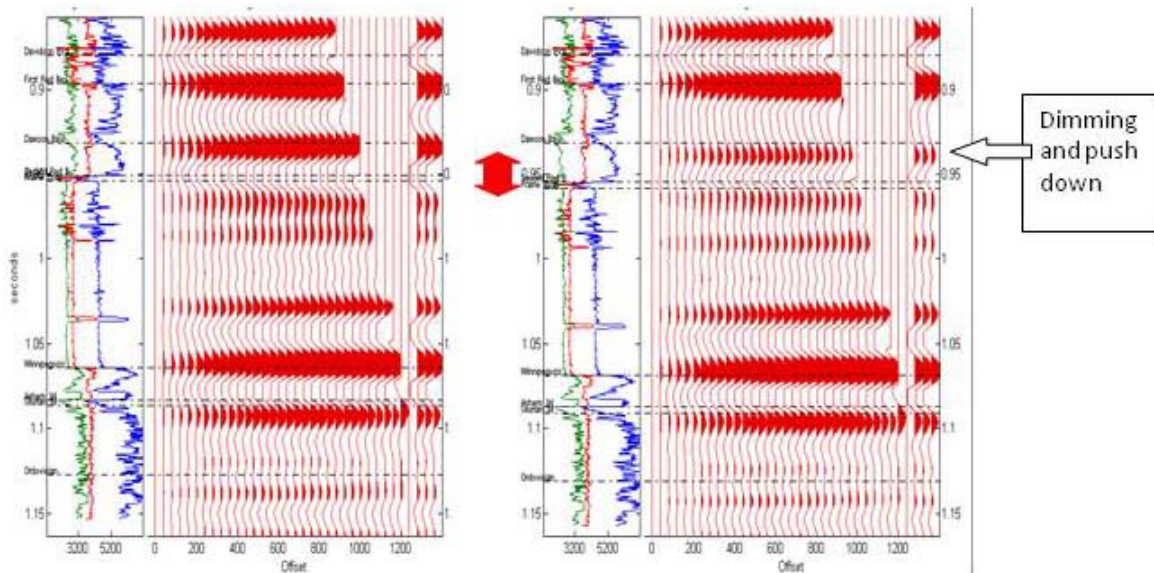


FIG. 19. Well logs (P velocity in blue, S-velocity in green, and density in red) and PS synthetic seismogram (NMO removed gather and summed response, duplicated 3 times) focusing on Dawson Bay and the Second Red Bed Shale for Well A. left: uncracked rock; right: cracked rock. The red arrow marks the strata cracked.

From the previous synthetic seismograms for Well A, we observe the following changes caused by cracks in the Dawson Bay and the Second Red Bed Shale:

- 1) Some push-down (time increase) in the PP wave and an amplitude versus offset (AVO) effect

- 2) Push-down and dimming (amplitude loss) in the PS wave
- 3) The effects are much stronger on the PS data

From the synthetic seismograms for Well B, we observe small AVO effects on the PP seismogram (Figure 20) and reflection character changes on PS response (Figure 21) over the cracked interval. Assuming that the PS data have the same frequency content as the PP data, amplitude dimming and push-down can be found on PS response (Figure 22), a strong PS change is observed.

We note that there may also be attenuation changes due to cracking and fluid saturation that would affect seismic waves. This might measurably affect the frequency content of the seismic waves and could be investigated in future work.

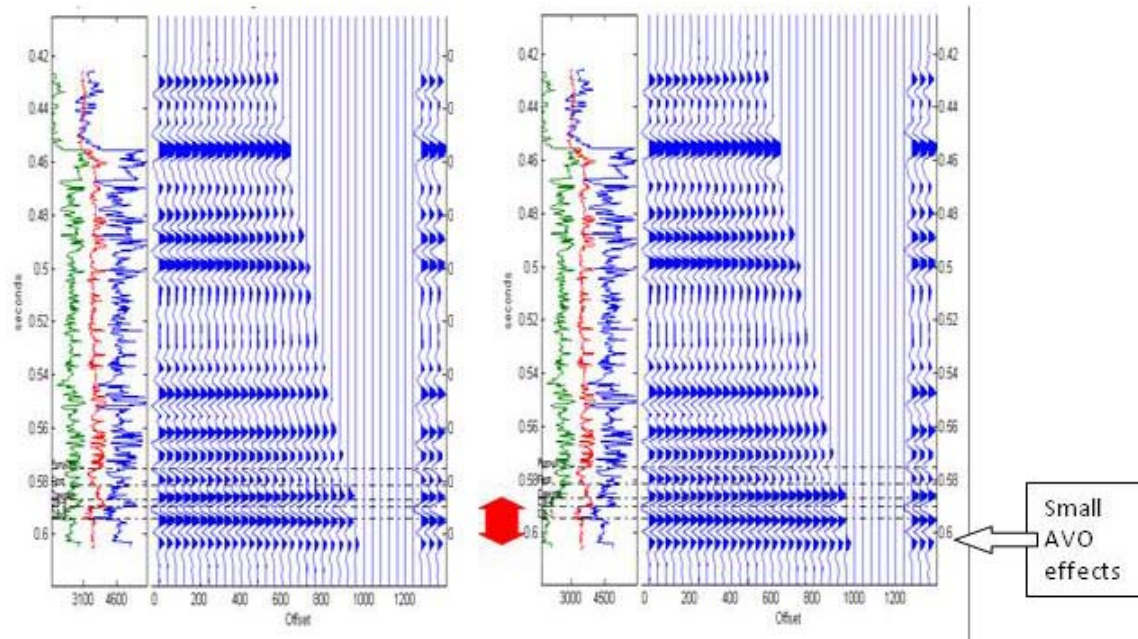


FIG. 20. Well logs (P velocity in blue, S-velocity in green, and density in red) and PP synthetic seismogram (NMO removed gather and summed response, duplicated 3 times) for Well B. Left: uncracked rock; right: cracked rock. The red arrow marks the strata cracked.

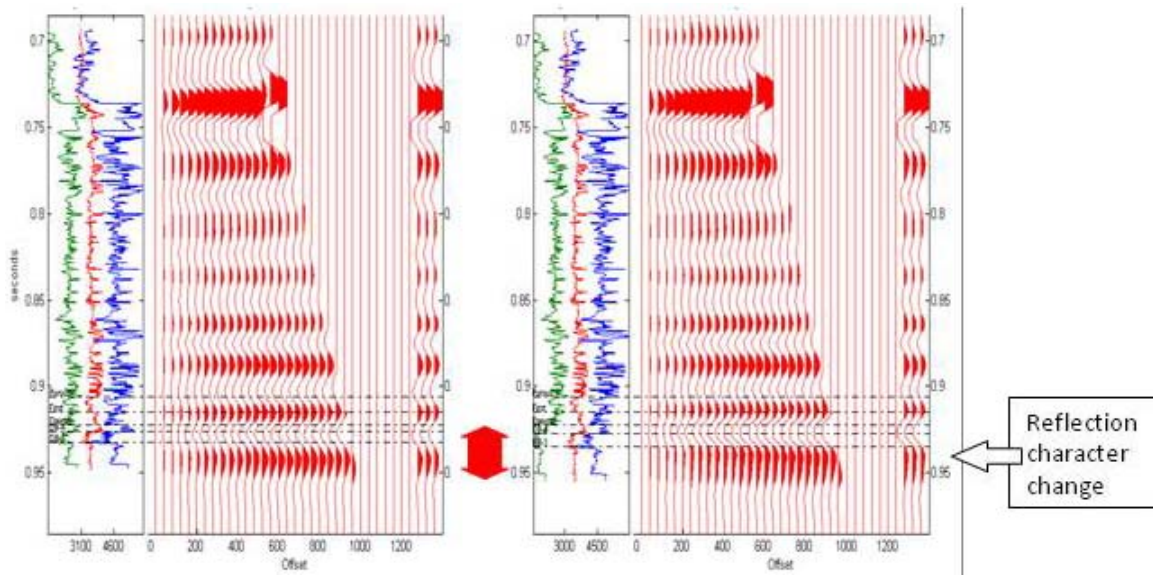


FIG. 21. Well logs (P velocity in blue, S-velocity in green, and density in red) and PS synthetic seismogram (NMO removed gather and summed response, duplicated 3 times) for Well B. Left: uncracked rock; right: cracked rock. The red arrow marks the strata cracked.

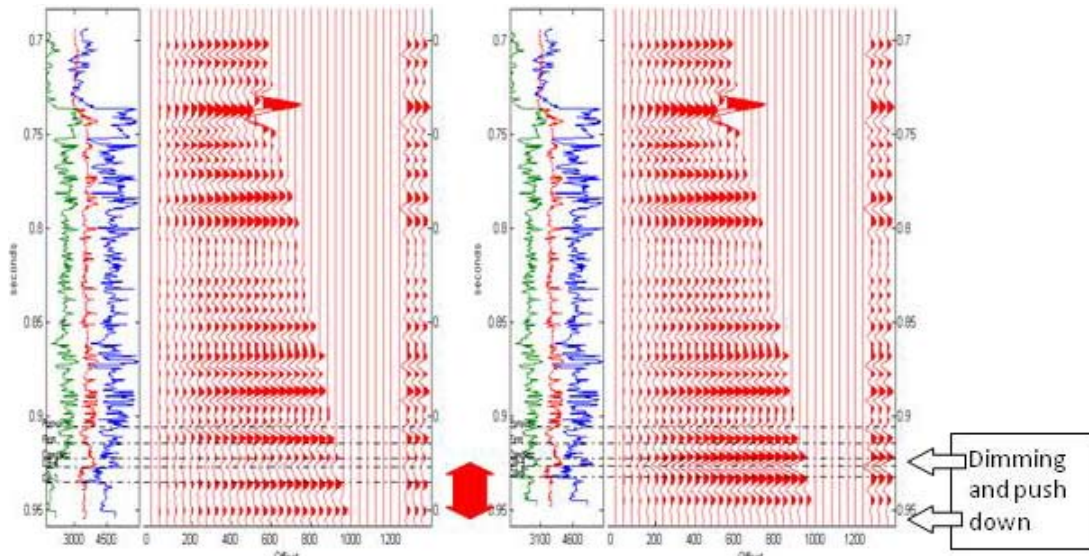


FIG. 22. Well logs (P velocity in blue, S-velocity in green, and density in red) and PS synthetic seismogram using wavelet with PP frequency content (NMO removed gather and summed response, duplicated 3 times) for Well B. Left: uncracked rock; right: cracked rock. The red arrow marks the strata cracked.

We now proceed to a preliminary correlation of the synthetic seismograms to some seismic data from the mining area. Because logs in Well A extend the deepest, we attempt to tie them to the only seismic data available to us (which is many kilometers distant from Well A). Somewhat surprisingly, there is a reasonable tie with P-wave synthetic seismograms to the PP field seismic section (Figure 23). Then, we tie our PS synthetic seismograms to the field PS seismic data (Figure 24). Again, a believable correlation. We note that there is a strong Dawson Bay reflection in the PS seismic

section. This bodes well for measuring changes in it. Finally, we correlate the PP and PS sections (Figure 25).

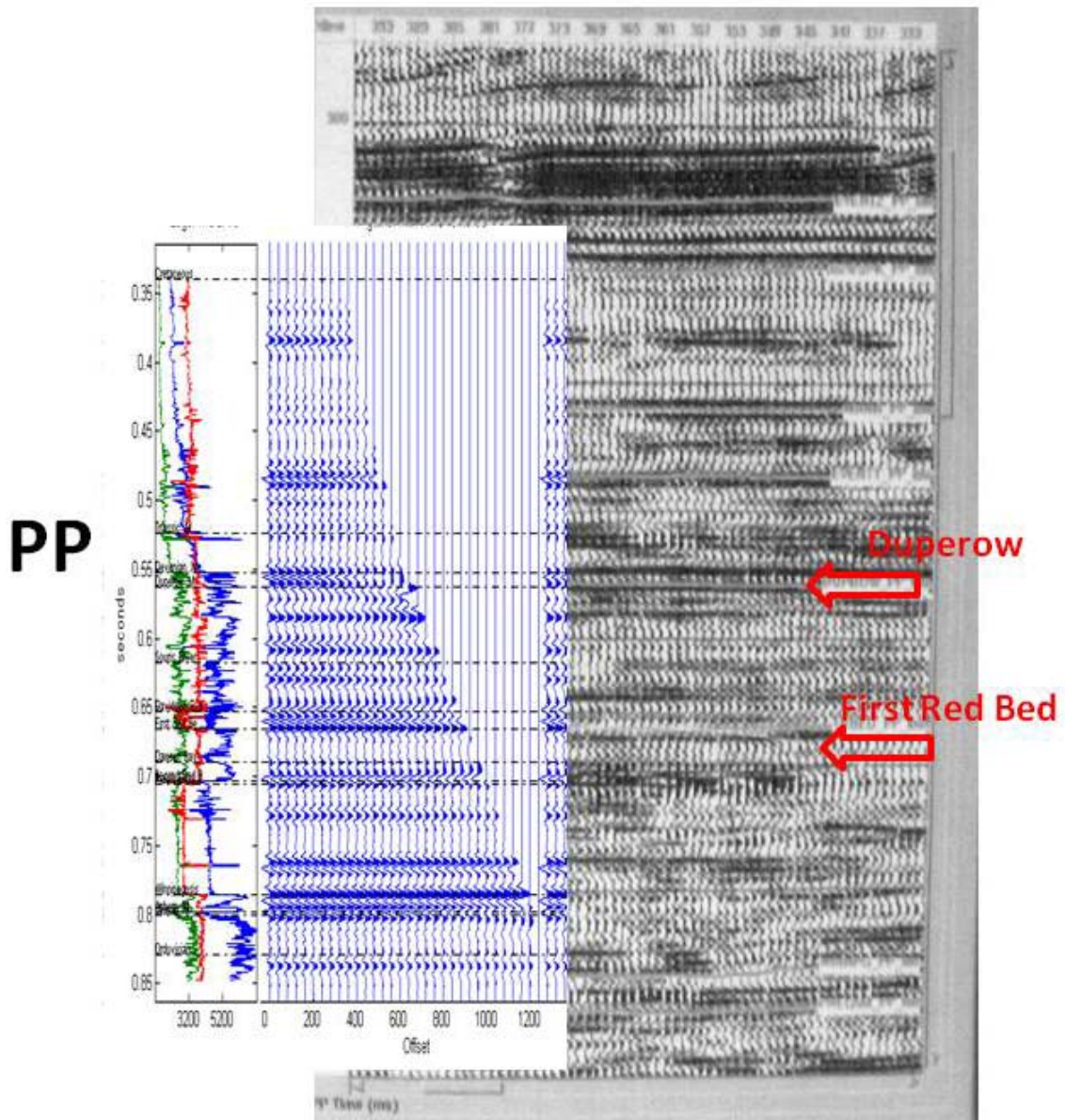


FIG. 23. Synthetic PP seismograms (blue, with well logs: P velocity in blue, S-velocity in green, and density in red) of Well A and Surface PP seismic data.

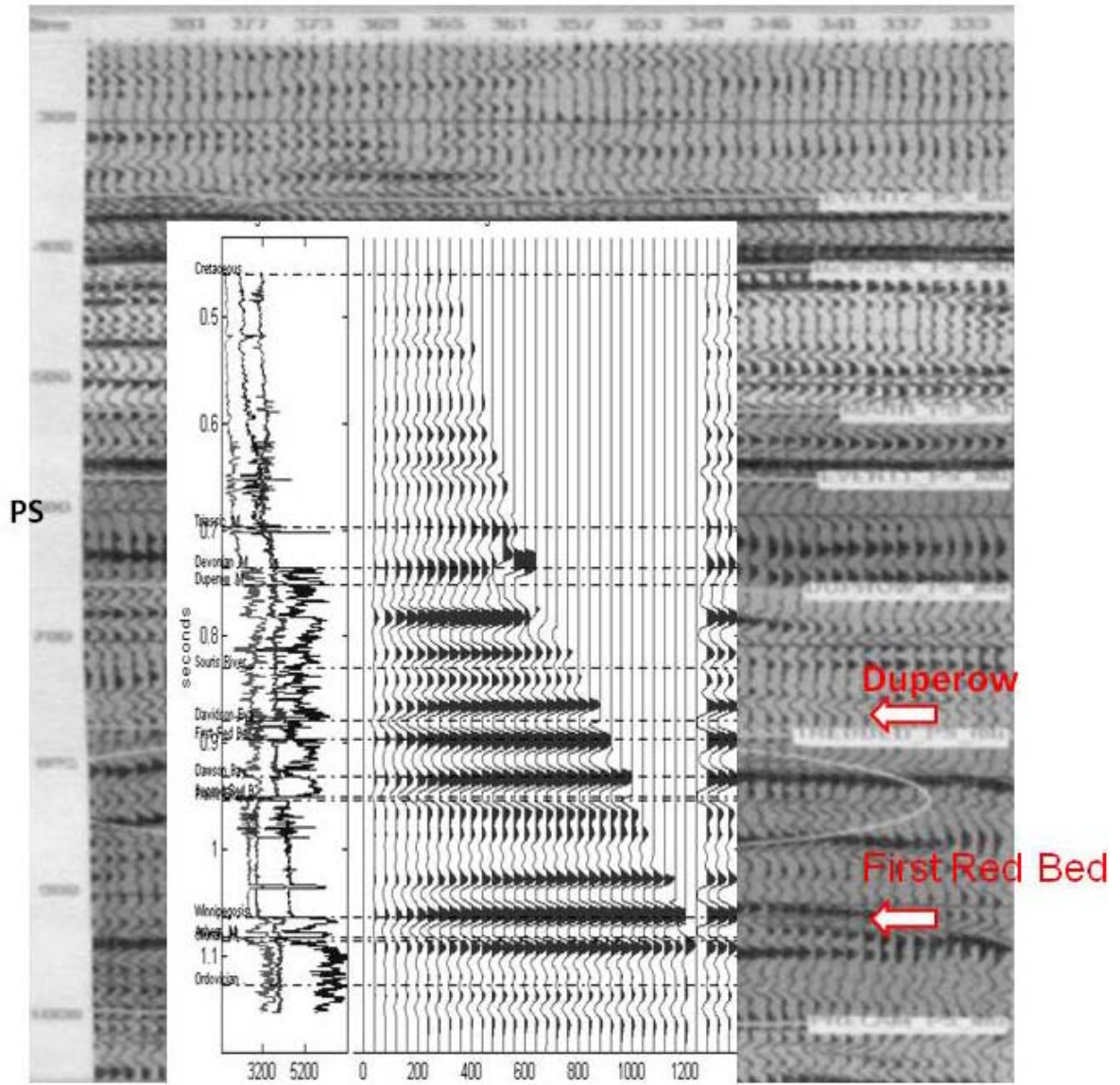


FIG. 24. Surface PS seismic data and synthetic PS seismograms (with well logs) of Well A.



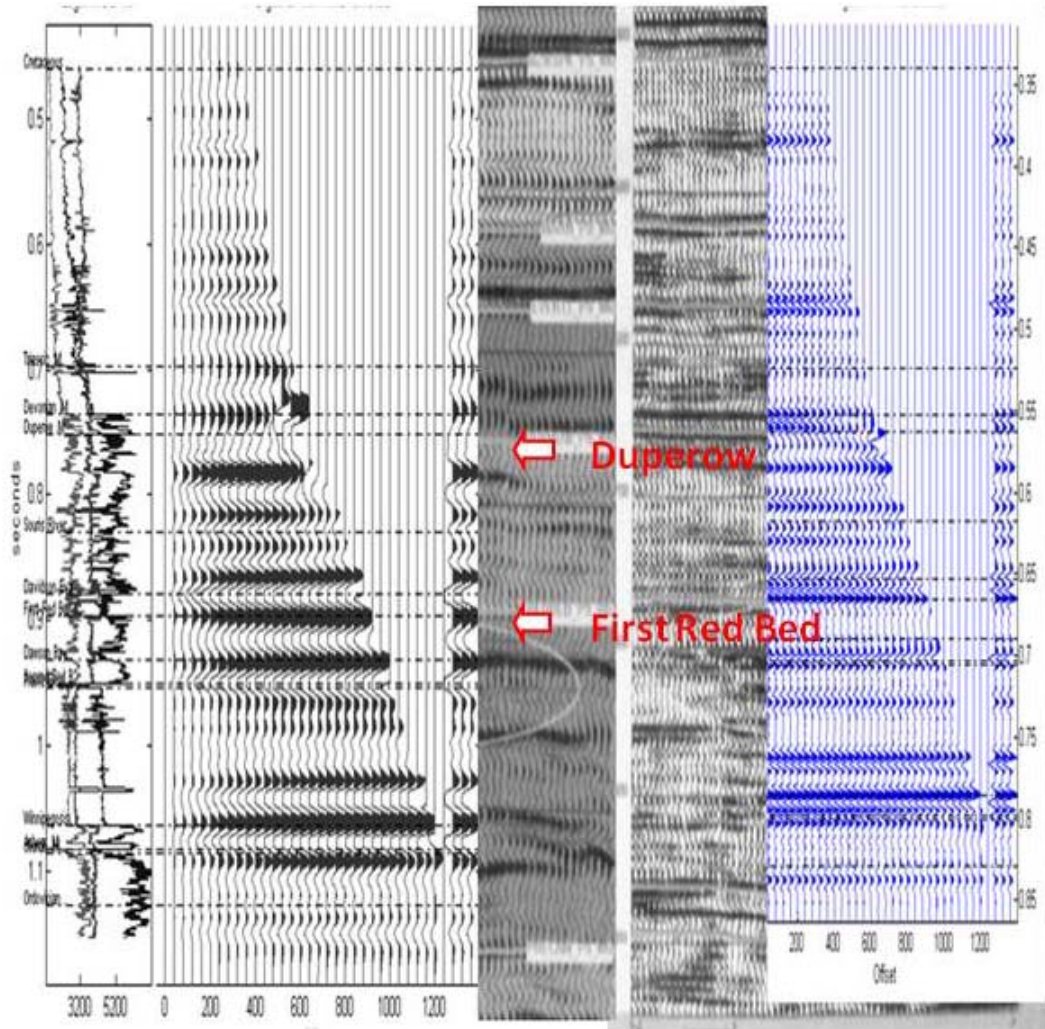


FIG. 25. Correlation of synthetic seismograms of Well A with surface seismic. From left to right: synthetic PP seismogram with well logs; PP surface seismic; synthetic PS seismogram; and PS surface seismic section.

A reasonable initial tie was found between the synthetic seismograms of Well A and the distant surface multi-component seismic data. We also have made an initial correlation between the synthetic PP seismogram from Well B and the surface PP seismic data in that area (Figure 26). There is a reasonable correlation. In general, the synthetic seismic data, which we have generated, correlates fairly well with the actual surface seismic data. This gives promise for further interpretation of the multicomponent seismic data and potential identification of cracked regions via anomalous responses or time-lapse differences.

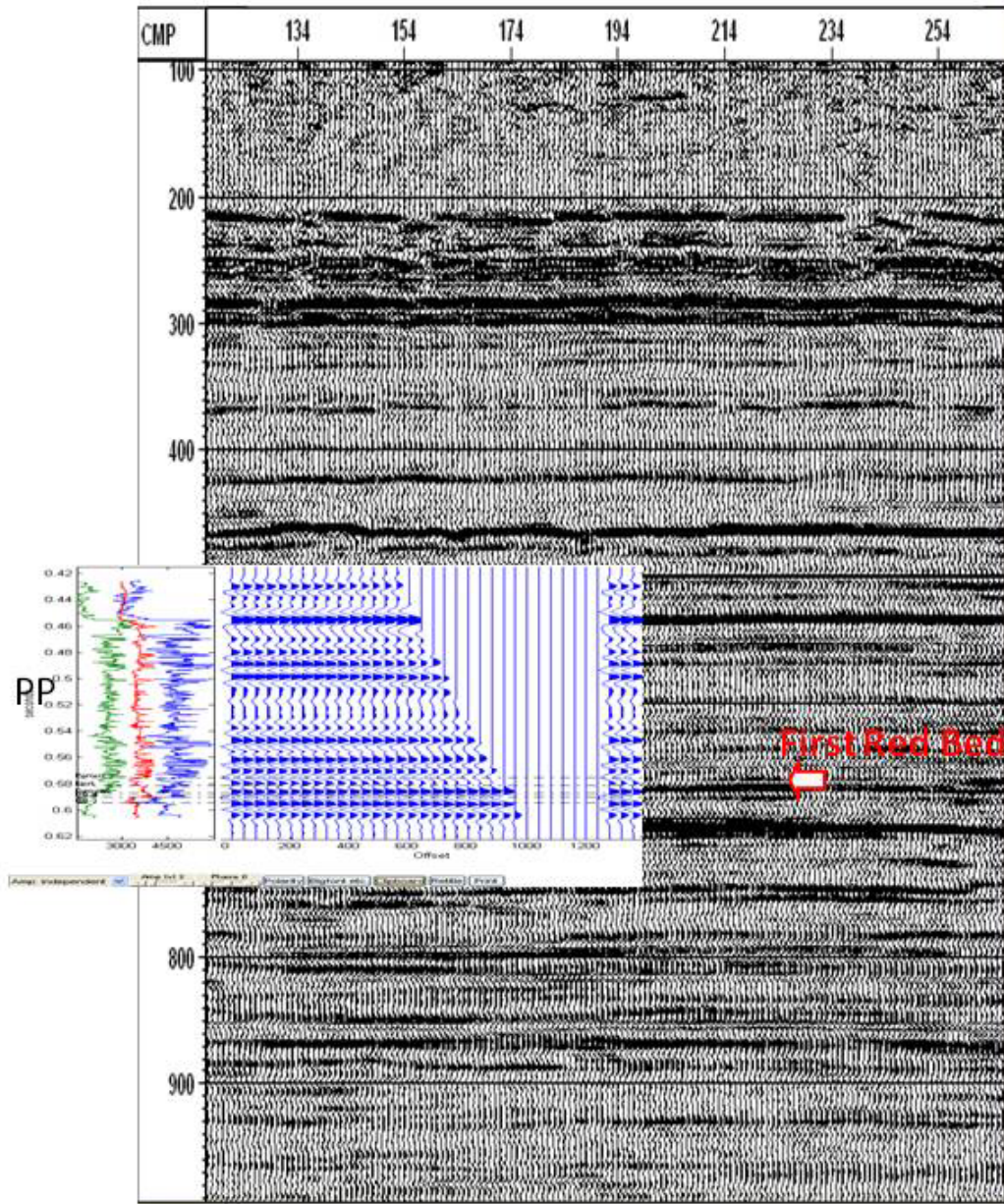


FIG. 26. Well logs (P velocity in blue, S-velocity in green, and density in red) and correlation between PP synthetic seismograms for Well B with surface PP seismic.

### SUMMARY

This report presents the results of a petrophysical and seismic simulation study in a potash mining area of western Canada. The goal of the work is to model the effects of cracked rocks in the Dawson Bay formation on seismic reflection character. Shear-wave sonic logs sometimes display unrealistic values. We can effectively edit these values, in this study, by using P velocity and density logs. Rock physics modeling (from Kuster-Toksöz and Hudson) indicates that P-wave and S-wave velocities will decrease (often significantly) with cracks or fractures. These cracked strata may also display various

types of anisotropy or velocity variation with direction. Synthetic seismogram calculation using the original log values and those with cracks shows observable changes. Those changes include “push-down” effects or time lags and amplitude variations with offset. The seismic character differences are especially evident in the PS reflections. The PP and PS synthetic seismograms correlate reasonably well, in initial correlations, with actual surface seismic sections. This indicates that multi-component seismic data are interpretable in, at least, this potash area of western Canada. This also suggests that by searching for anomalies in the multi-component seismic data or by looking for changes in repeated seismic surveys, we may be able to detect cracks in the Dawson Bay and similar intervals.

### ACKNOWLEDGEMENTS

Support by CREWES sponsors is gratefully appreciated.

### REFERENCES

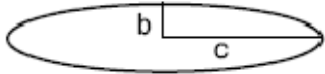
- Berryman, J.G., 1980. Long-wavelength propagation in composite elastic media. *J. Acoust. Soc. Am.*, **68**, 1809-1831.
- Brown, R., and Korringa, J., 1975. On the dependence of the elastic properties of a porous rock on the compressibility of the pore fluid. *Geophysics*, **40**, 606-616.
- Crain, R., 2005, Well logging course notes. *Geophysics* 449, University of Calgary.
- DeMille, G., Shouldice, J.R., and Nelson, H.W., 1964, Collapse structure related to evaporites of the Prairie Formation, Saskatchewan; *Geol. Soc. Amer. Bull.*, **75**, 307-316.
- Fuzesy, L.M., 1982, Petrology of potash ore in the Esterhazy Member of the Middle Devonian Prairie Evaporite in southeastern Saskatchewan, *Proceedings of the Fourth International Williston Basin Symposium*, 67-73.
- Gendzwill, D. J. and Lundberg, R. M., 1989, Seismic anomalies of Saskatchewan Winnipegosis mounds: *Geophysical Atlas of Western Canada Hydrocarbon Reservoirs: Canadian Society of Exploration Geophysicists*.
- Han, D.H., and Batzle, M., 2004, Estimating shear velocity based on dry P-wave and shear modulus relationship, *SEG expanded abstracts*.
- Hamid, H., Morozov, I.B., and Kreis, L.K., 2004. Progress in seismic delineation of the southern margin of the Middle Devonian Prairie Evaporite Formation in the Elk Point Basin, south-central Saskatchewan. *Summary of Investigations 2004, Volume 1, Saskatchewan Geological Survey, Sask. Industry Resources, Misc. Rep. 2004-4.1, CD-ROM, Paper A-5, 9p.*
- Hudson, J.A., 1981. Wave speeds and attenuation of elastic waves in material containing cracks. *Geophys. J. Royal Astronom. Soc.* **64**, 133-150.
- Kuster, G.T., and Toksöz, M.N., 1974, Velocity and attenuation of seismic waves in two-phase media: Part I. theoretical formulations. *Geophysics*, **39**, 587-606.
- Mavko, G., Mukerji, T., and Dvorkin, J., 1998, *The rock physics handbook*, Cambridge University Press.
- Mavko, G., 2006, Introduction to Rock Physics course notes: Stanford University.

- Maxwell, M., Unrau, J., Eso, R. A., Oldenburg, D.W., Song, L.P., 2005, Advancement of 2D and 3D electrical resistivity techniques for underground applications in a potash mine: Technical Paper, International Symposium on Mine Planning and Equipment Selection, Banff, 2005.
- Prugger, A., Nemeth, B., and Danyluk, T., 2004, Detailed 3D seismic imaging of Paleozoic Karst / collapse disturbances in Saskatchewan: Case Study from the Potash Belt. CSEG Expanded Abstracts.
- Zhang, Z., and Stewart, R.R., 2008, Rock physics models for cracked media, **20**: CREWES Research Report.

### APPENDIX - CRACK DESCRIPTION

There are several parameters often used to describe simplified versions of a cracked rock:

The quantity  $\alpha=b/c$  is called the aspect ratio.



The crack density is the number of cracks per unit volume:  $\epsilon = \frac{Nc^3}{V_{bulk}}$

where

$N$ : number of cracks in volume  $V_{bulk}$ ;

$c$ : semi-major axis value of cracks.

If we assume a rock contains  $N/V_b$  thin oblate spheroidal cracks per unit bulk volume, each having semi-major axis and semi-minor axis  $b=\alpha c$ , where  $\alpha$  is the aspect ratio, the crack porosity will be:

$$\phi = \frac{N}{V_b} \frac{4\pi c^2 b}{3} = \frac{N}{V_b} \frac{4\pi c^3 \alpha}{3}$$

Where  $N$  is the number of cracks in volume  $V_b$ ;  $c$ : semi-major axis value of cracks;  $\alpha$ : aspect ratio.

Thus, crack density is:

$$\epsilon = \frac{N}{V} c^3 = \frac{3\phi}{4\pi\alpha}$$